Visual Space Distortion

Cornelia Fermüller, LoongFah Cheong, and
Yiannis Aloimonos

Computer Vision Laboratory
Center for Automation Research
University of Maryland
College Park, MD 20742-3275

Abstract

We are surrounded by surfaces that we perceive by visual means. Understanding the basic principles behind this perceptual process is a central theme in visual psychology, psychophysics and computational vision. In many of the computational models employed in the past, it has been assumed that a metric representation of physical space can be derived by visual means. Psychophysical experiments, as well as computational considerations, can convince us that the perception of space and shape has a much more complicated nature, and that only a distorted version of actual, physical space can be computed. This paper develops a computational geometric model that explains why such distortion might take place. The basic idea is that, both in stereo and motion, we perceive the world from multiple views. Given the rigid transformation between the views and the properties of the image correspondence, the depth of the scene can be obtained. Even a slight error in the rigid transformation parameters causes distortion of the computed depth of the scene. The unified framework introduced here describes this distortion in computational terms. We characterize the space of distortions by its level sets, that is, we characterize the systematic distortion via a family of iso-distortion surfaces which describes the locus over which depths are distorted by some multiplicative factor. Given that humans' estimation of egomotion or estimation of the extrinsic parameters of the stereo apparatus is likely to be imprecise, the framework is used to explain a number of psychophysical experiments on the perception of depth from motion or stereo.

The support of the Office of Naval Research under Grant N00014-96-1-0587 is gratefully acknowledged. The second author was also supported in part by the Tan Kah Khee Postgraduate Scholarships. Special thanks to Sara Larson for her editorial and graphics assistance.

1 Introduction

The nature of the representation of the world inside our heads as acquired by visual perception has persisted as a topic of investigation for thousands of years, from the works of Aristotle to the present [26]. In our day, answers to this question have several practical consequences in the field of robotics and automation. An artificial system equipped with visual sensors needs to develop representations of its environment in order to interact successfully with it. At the same time, understanding the way space is represented in the brains of biological systems is key to unraveling the mysteries of perception. We refer later to space represented inside a biological or artificial system as *perceptual space*, as opposed to *physical*, extra-personal *space*.

Interesting non-computational theories of perceptual space have appeared over the years in the fields of philosophy and cognitive science [22]. Computational theories, on the other hand, developed during the past thirty years in the area of computer vision, have followed a brute-force approach, equating physical space with perceptual space. Euclidean geometry involving metric properties has been used very successfully in modeling physical space. Thus, early attempts at modeling perceptual space concentrated on developing metric three-dimensional descriptions of space, as if it were the same as physical space. In other words, perceptual space was modeled by encoding the exact distances of features in three dimensions. The apparent ease with which humans perform a plethora of vision-guided tasks creates the impression that humans, at least, compute representations of space that have a high degree of generality; thus, the conventional wisdom that these descriptions are of a Euclidean metric nature was born and has persisted until now [1, 17, 26].

Computational considerations, however, can convince us that for a monocular or a binocular system moving in the world it is not possible to estimate an accurate description of three-dimensional metric structure, i.e., the exact distances of points in the environment from the nodal point of the eye or camera. This paper explains this in computational terms for the case of perceiving the world from multiple views. This includes the cases of both motion and stereo. Given two views of the world, whether these are the left and right views of a stereo system or successive views acquired by a moving system, the depth of the scene in view depends on two factors: (a) the three-dimensional rigid transformation between the views, hereafter called the *3D transformation*, and (b) the identification of image features in the two views that correspond to the same feature in the 3D world, hereafter called *visual correspondence*.

If there were no errors in the 3D transformation or the visual correspondence, then clearly the depth of the scene in view could be accurately recovered and thus a metric description could be obtained for perceptual space. Unfortunately, this is never the case. In the case of stereo, the 3D transformation amounting to the extrinsic calibration parameters of the stereo rig cannot be accurately estimated, only approximated [7]. In the case of motion, the three-dimensional motion parameters describing rotation and translation are estimated within error bounds [4, 5, 6, 8, 27, 33]. Finally, visual correspondence itself cannot be obtained perfectly; errors are always present. Thus, because of errors in both visual correspondence and 3D transformation, the recovered depth of the scene is always a *distorted* version of the scene structure. The fundamental contribution of this paper is the development of a computational framework showing the geometric laws under which the recovered scene shape is distorted. In other words, there is a systematic way in which visual space is distorted; the transformation from physical to perceptual space belongs to the family of Cremona transformations [30].[1]

The power of the computational framework we introduce is demonstrated by using it to explain recent results in psychophysics. A number of recent psychophysical experiments have shown that humans make incorrect judgments of depth using either stereo [13, 18] or motion [15, 31]. Our computational theory explains these psychophysical results and demonstrates that, in general, perceived space is not describable using a well-established geometry such as hyperbolic, elliptic, affine or projective. Understanding the invariances of distorted perceived space will contribute to the understanding of robust representations of shape and space, with many consequences for the problem of recognition. This work was motivated by our recent work on direct perception and qualitative shape representation [10, 11] and was inspired by the work of Koenderink and van Doorn on pictorial relief [21].

In the psychophysical literature it has been argued before for the interpretation of stereo data that an incorrect estimation of the viewing geometry causes incorrect estimation of the depth of the scene. This was first hypothesized but not further elaborated on by Helmholtz [34] and was explained by means of a number of tasks involving depth judgments from stereo by Foley [13]. In this paper we provide a general framework of space distortion on the basis of incorrect estimation of viewing geometry which can be used to explain estimation from motion as well as stereo. In our exposition we concentrate primarily on the experiments described in [31], which are concerned with both motion and stereo, and we use these experiments to explain in detail the utilization of the iso-distortion framework. In these experiments Tittle et al. tested how orientations of objects in space and absolute distance influence the judgment of depth, and they found very different results from the motion and stereo cues. The experiments were cleverly designed so that the underlying geometries of the motion and stereo configurations are qualitatively similar. Thus they are of great comparative interest. We also discuss an additional motion experiment [15] and some well known stereo experiments.

The computational arguments presented here are based on two ideas. First, the 2D image representation derived for stereo perception is of a different nature than the one derived for motion perception. Second, the only thing assumed about the scene is that it lies in front of the image plane, and thus all depth estimates have to be positive; therefore, the perceptual system, when estimating 3D motion, minimizes the number of image points whose corresponding scene points have negative depth values due to errors in the estimate of the motion. In [9] an error analysis has been performed to study the optimal relationship between translational and rotational errors which leads to this minimization. It has been found that for a general motion imaged on a plane the projection of the translational error motion vector and the projection of the rotational error motion vector must have a particular relationship. Furthermore, the relative amount

[1] In the projective plane, a transformation $(x,y,z) \rightarrow (x',y',z')$ with $\rho x' = \phi_1(x,y,z)$, $\rho y' = \phi_2(x,y,z)$, $\rho z' = \phi_3(x,y,z)$ where ϕ_1, ϕ_2, ϕ_3 are homogeneous polynomials and ρ any scalar, is called a rational transformation. A rational transformation whose inverse exists and is also rational is called a Cremona transformation.

of translational and rotational error can be evaluated as a function of scene structure. These findings are utilized in the explanation of the psychophysical experiments.

The organization of this paper is as follows. Section 2.1 introduces the concept of iso-distortion surfaces. Considering two close views, arising from a system in general rigid motion, we relate image motion measurements to the parameters of the 3D rigid motion and the depth of the scene. Then, assuming that there is an error in the rigid motion parameters, we find the computed depth as a function of the actual depth and the parameters of the system. Considering the points in space that are distorted by the same amount, we find them to lie on surfaces that in general are hyperboloids. These are the iso-distortion surfaces that form the core of our approach. In Section 2.2 we further describe the iso-distortion surfaces in both 3D and visual space and we introduce the concept of the holistic or H-surfaces. These are surfaces that describe all iso-distortion surfaces distorted by the same amount, irrespective of the direction (n_x, n_y) in the image in which measurements of visual correspondence are made. The H-surfaces are important in our analysis of the case of motion since measurements of local image motion can be in any direction and not just along the horizontal direction which is dominant in the case of stereo. Section 3 describes psychophysical experiments from the recent literature using motion and stereo, and Section 4 explains their results using the iso-distortion framework. Section 4.1 describes in detail the coordinate systems and the underlying rigid transformations for the specific experiments. Sections 4.2 and 4.3 explain the experimental results of [31] for motion and stereo respectively, and Section 4.4 discusses the experimental results of the additional purely motion or stereo experiments using the framework introduced here. Section 5 concludes the paper and discusses the relationship of this work to other attempts in the literature to capture the essence of perceptual space.

2 Distortion of Visual Space

2.1 Iso-distortion Surfaces

As an image formation model, we use the standard model of perspective projection on the plane, with the image plane at a distance f from the nodal point parallel to the XY plane, and the viewing direction along the positive Z axis as illustrated in Figure 1. We want a model that can be used both for motion and stereo. Thus, we consider a differential model of rigid motion. This model is valid for stereo, which constitutes a special constrained motion, when making the small baseline approximation that is used widely in the literature [21].

Specifically, we model the change of viewing geometry differentially through a rigid motion with translational velocity (U, V, W) and rotational velocity (α, β, γ) of the observer in the coordinate system $OXYZ$. Stereo can be approximated as a constrained rigid motion with translation $(U, 0, W)$ and rotation $(0, \beta, 0)$, as explained in detail in Section 4.1. In the case of stereo the measurements obtained on the image are the so-called disparities which we approximate here through a continuous flow field. As, due to the stereo viewing geometry, the disparities are close to horizontal, in the forthcoming analysis we only employ horizontal image flow measurements. On the other hand, in the case of continuous motion from local image information only the component of the flow

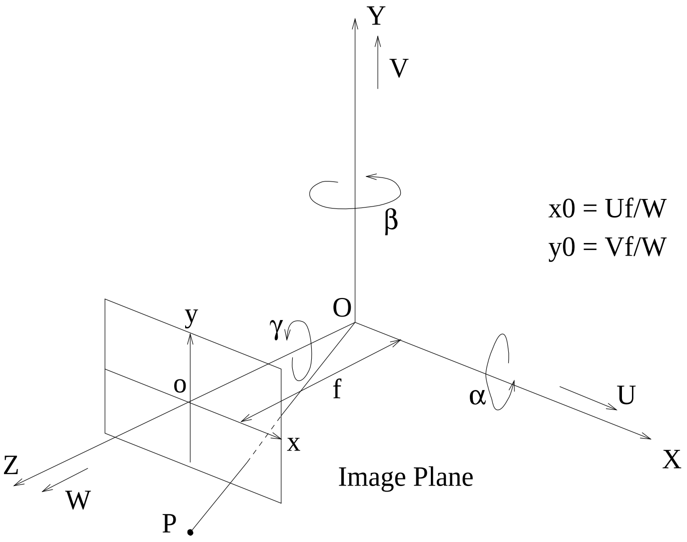

Figure 1: The image formation model. $OXYZ$ is a coordinate system fixed to the camera. O is the optical center and the positive Z axis is the direction of view. The image plane is located at a focal length f pixels from O along the Z axis. A point P at (X, Y, Z) in the world produces an image point p at (x, y) on the image plane where (x, y) is given by $\left(\frac{fX}{Z}, \frac{fY}{Z}\right)$. The instantaneous motion of the camera is given by the translational vector (U, V, W) and the rotational vector (α, β, γ).

perpendicular to edges (along image gradients) can, in general, be obtained. Thus, in the case of motion, we consider as input the field resulting from this component, which is known as the normal flow field. In summary, for both cases of stereo and motion we use the projection of the flow field on orientations (n_x, n_y), which in the case of motion represent image gradients while in the case of stereo represent horizontal directions.

As is well known, from the 2D image measurements alone as a consequence of the scaling ambiguity, only the direction of translation $(x_0, y_0) = \left(\frac{U}{W}f, \frac{V}{W}f\right)$ represented in the image plane by the epipole (also called the FOE (focus of expansion) or FOC (focus of contraction) depending on whether W is positive or negative), the scaled depth Z/W and the rotational parameters can possibly be obtained from flow measurements. Using this notation the equations relating the 2D velocity $\mathbf{u} = (u, v) = (u_{\text{trans}} + u_{\text{rot}}, v_{\text{trans}} + v_{\text{rot}})$ of an image point to the 3D velocity and the depth of the corresponding scene point are

$$\begin{aligned} u &= u_{\text{trans}} + u_{\text{rot}} = (x - x_0)\frac{W}{Z} + \alpha xy - \beta\left(\frac{x^2}{f} + f\right) + \gamma y \\ v &= v_{\text{trans}} + v_{\text{rot}} = (y - y_0)\frac{W}{Z} + \alpha\left(\frac{y^2}{f} + f\right) - \frac{\beta xy}{f} - \gamma x \end{aligned} \tag{1}$$

where $u_{\text{trans}}, v_{\text{trans}}$ are the horizontal and vertical components of the flow due to translation, and $u_{\text{rot}}, v_{\text{rot}}$ the horizontal and vertical components of the flow due to rotation, respectively.

The velocity component $\mathbf{u}_n$ of the flow in any direction $\mathbf{n} = (n_x, n_y)$ has value

$$u_n = un_x + vn_y. \tag{2}$$

Knowing the parameters of the viewing geometry exactly, the scaled depth can be derived from (2). Since the depth can only be derived up to a scale factor, we set $W = 1$ and obtain

$$Z = \frac{(x - x_0)n_x + (y - y_0)n_y}{u_n - u_{\mathrm{rot}} n_x - v_{\mathrm{rot}} n_y}$$

If there is an error in the estimation of the viewing geometry, this will in turn cause errors in the estimation of the scaled depth, and thus a distorted version of space will be computed. In order to capture the distortion of the estimated space, we describe it through surfaces in space which are distorted by the same multiplicative factor, the so-called iso-distortion surfaces. To distinguish between the various estimates, we use the hat sign " ˆ " to represent estimated quantities, the unmarked letters to denote the actual quantities, and the subscript "ϵ" to represent errors, where the estimates are related as follows:

$$\begin{aligned}
(\hat{x_0}, \hat{y_0}) &= (x_0 - x_{0_\epsilon}, y_0 - y_{0_\epsilon}) \\
(\hat{\alpha}, \hat{\beta}, \hat{\gamma}) &= (\alpha - \alpha_\epsilon, \beta - \beta_\epsilon, \gamma - \gamma_\epsilon) \\
\hat{\mathbf{u}}_{\mathrm{rot}} &= (\hat{u}_{\mathrm{rot}}, \hat{v}_{\mathrm{rot}}) = \mathbf{u}_{\mathrm{rot}} - \mathbf{u}_{\mathrm{rot}_\epsilon} = (u_{\mathrm{rot}} - u_{\mathrm{rot}_\epsilon}, v_{\mathrm{rot}} - v_{\mathrm{rot}_\epsilon})
\end{aligned}$$

If we also allow for a noise term N in the estimate $\hat{u}_n$ of the component flow u_n, we have $\hat{u}_n = u_n + N$. The estimated depth becomes

$$\begin{aligned}
\hat{Z} &= \frac{(x - \hat{x}_0)n_x + (y - \hat{y}_0)n_y}{\hat{u}_n - (\hat{u}_{\mathrm{rot}} n_x + \hat{v}_{\mathrm{rot}} n_y)} \qquad \text{or} \\
\hat{Z} &= Z \cdot \left(\frac{(x - \hat{x}_0)n_x + (y - \hat{y}_0)n_y}{(x - x_0)n_x + (y - y_0)n_y + Z(u_{\mathrm{rot}_\epsilon} n_x + v_{\mathrm{rot}_\epsilon} n_y) + NZ} \right) \qquad (3)
\end{aligned}$$

From (3) we can see that $\hat{Z}$ is obtained from Z through multiplication by a factor given by the term inside the brackets, which we denote by D and call the distortion factor. In the forthcoming analysis we do not attempt to model the statistics of the noise and we will therefore ignore the noise term. Thus, the distortion factor takes the form

$$D = \frac{(x - \hat{x}_0)n_x + (y - \hat{y}_0)n_y}{\begin{array}{l}(x - x_0)n_x + (y - y_0)n_y \\ +Z\left[\left(\frac{\alpha_\epsilon xy}{f} - \beta_\epsilon\left(\frac{x^2}{f} + f\right) + \gamma_\epsilon y\right) n_x + \left(\alpha_\epsilon\left(\frac{y^2}{f} + f\right) - \beta_\epsilon \frac{xy}{f} - \gamma_\epsilon x\right) n_y\right]\end{array}} \qquad (4)$$

or, in a more compact form

$$D = \frac{(x - \hat{x}_0)\, n_x + (y - \hat{y}_0)\, n_y}{(x - x_0 + Z u_{\mathrm{rot}_\epsilon})\, n_x + (y - y_0 + Z v_{\mathrm{rot}_\epsilon})\, n_y}$$

Equation (4) describes, for any fixed direction (n_x, n_y) and any fixed distortion factor D, a surface $f(x, y, Z) = 0$ in space, which we call an iso-distortion surface. For specific values of the parameters $x_0, y_0, \hat{x}_0, \hat{y}_0, \alpha_\epsilon, \beta_\epsilon, \gamma_\epsilon$ and (n_x, n_y), this iso-distortion surface has the obvious property that points lying on it are distorted in depth by the same multiplicative factor D. Also, from (3) it follows that the transformation from perceptual to physical space is a Cremona transformation.

It is important to realize that, on the basis of the preceding analysis, the distortion of depth also depends upon the direction (n_x, n_y) and is therefore different for different directions of flow in the image plane. This means simply that if one estimates depth from optical flow in the presence of errors, the results can be very different depending on whether the horizontal, vertical, or any other component is used; depending on the direction, any value between $-\infty$ and $+\infty$ can be obtained! It is therefore imperative that a good understanding of the distortion function be obtained, before visual correspondences are used to recover the depth or structure of the scene.

In order to derive the iso-distortion surfaces in 3D space we substitute $x = \frac{fX}{Z}$ and $y = \frac{fY}{Z}$ in (4), which gives the following equation:

$$\begin{aligned} D\left(\left(\alpha_\epsilon XY - \beta_\epsilon\left(X^2+Z^2\right) + \gamma_\epsilon YZ\right) n_x + \left(\alpha_\epsilon\left(Y^2+Z^2\right) - \beta_\epsilon XY - \gamma_\epsilon XZ\right) n_y\right) \\ - \quad \left(X - \frac{\hat{x}_0 Z}{f} - D\left(X - \frac{x_0 Z}{f}\right)\right) n_x - \left(Y - \frac{\hat{y}_0 Z}{f} - D\left(Y - \frac{y_0 Z}{f}\right)\right) n_y = 0 \end{aligned}$$

describing the iso-distortion surfaces as quadratic surfaces—in the general case, as hyperboloids. One such surface is depicted in Figure 2. Throughout the paper we will need access to the iso-distortion surfaces from two points of view. On the one hand we want to compare surfaces corresponding to the same D, but different gradient directions; thus we are interested in the families of D iso-distortion surfaces (see Figure 3a). On the other hand we want to look at surfaces corresponding to the same gradient direction $\mathbf{n}$, but different D's, the families of $\mathbf{n}$ iso-distortion surfaces (see Figure 3b). We will also be interested in the intersections of the surfaces with planes parallel to the XZ, YZ, and XY planes. These intersections give rise to families of iso-distortion contours; for an example see Figure 4.

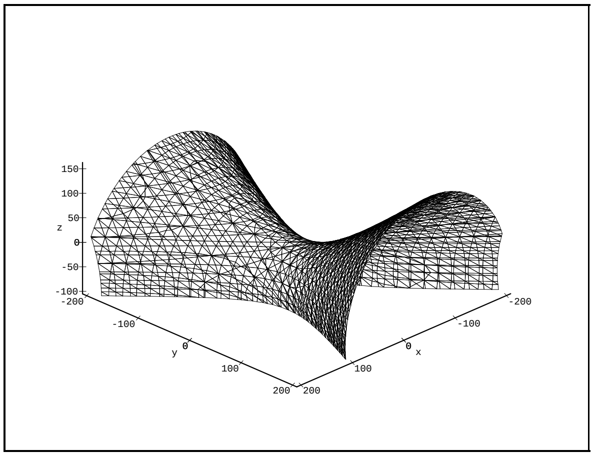

Figure 2: Iso-distortion surface in XYZ space. The parameters are: $x_0 = 10$, $x_{0_\epsilon} = -1$, $y_0 = -25$, $y_{0_\epsilon} = -5$, $\alpha_\epsilon = -0.05$, $\beta_\epsilon = -0.1$, $\gamma_\epsilon = -0.005$, $f = 1$, $D = 1.5$, $n_x = 0.7$.

2.2 Visualization of Iso-distortion Surfaces

The iso-distortion surfaces presented in the previous section were developed for the general case, i.e., when the 3D transformation between the views is a general rigid motion.

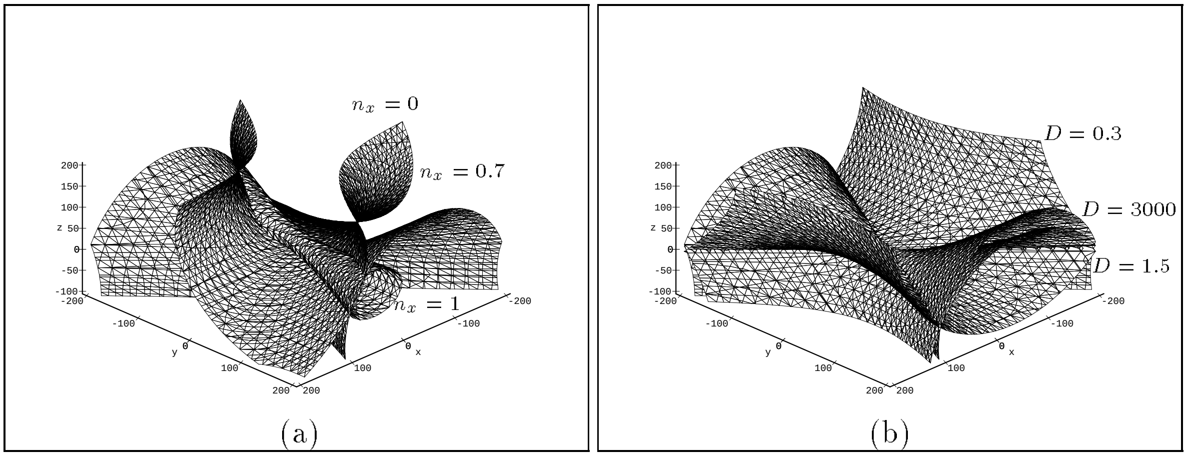

Figure 3: (a) Family of D iso-distortion surfaces for $n_x = 1, 0.7, 0$. (b) Family of $\mathbf{n}$ iso-distortion surfaces for $D = 0.3, 3000, 1.5$. The other parameters are as in Figure 2.

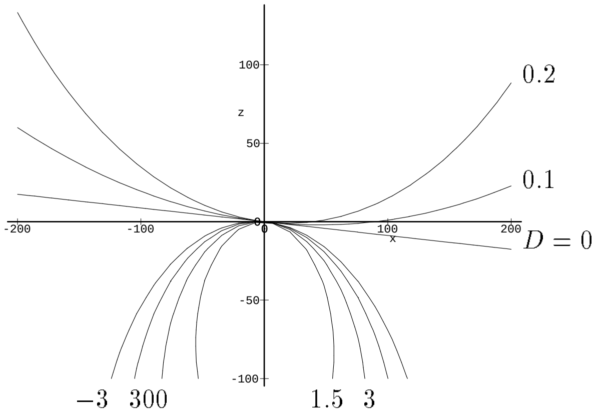

Figure 4: Intersection of a family of $\mathbf{n}$ iso-distortion surfaces (as shown in Figure 3b) with the XZ plane gives rise to a family of iso-distortion contours.

However, the psychophysical experiments that we will explain in the sequel considered constrained motion: rotation only around the Y axis and translation only in the XZ plane. The only motion parameters to be considered are therefore β_ϵ, x_0 and $\hat{x}_0$, and the iso-distortion surfaces become

$$D\beta_\epsilon X^2 n_x + D\beta_\epsilon Z^2 n_x + D\beta_\epsilon XY n_y - (D-1)\,X n_x - (D-1)\,Y n_y - (\hat{x}_0 - D x_0)\,\frac{n_x}{f} Z = 0$$

which in general constitute hyperboloids. For horizontal flow vectors ($n_x = 1, n_y = 0$) they become elliptic cylinders and for vertical flow vectors they become hyperbolic cylinders.

Figure 5 provides an illustration of an iso-distortion surface for a general flow direction (here $n_x = 0.7$, $n_y = 0.714$). For our purposes, only the parts of the iso-distortion surfaces within the range visible from the observer are of interest. Since in the motion considered later the FOE has a large value, these parts show very little curvature and appear to be close to planar, as can be seen from Figure 5b.

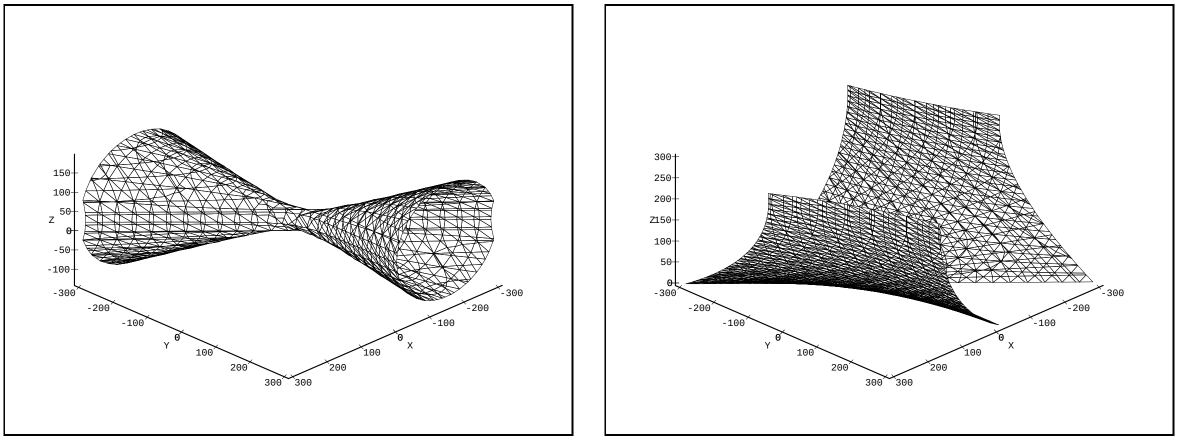

(a)

(b)

Figure 5: (a) A general iso-motion surface in 3D space. The Z axis corresponds to the optical axis. (b) Section of an iso-motion surface for a limited field of view in front of the image plane for large values of x_0.

In order to make it easier to grasp the geometrical organization of the iso-distortion surfaces we next perform a simplification and use in addition to 3D space also visual space (that is, xyZ space): Within a limited field of view, terms quadratic in the image coordinates are small relative to linear and constant terms; thus we ignore them for the moment, which simplifies the rotational term for the motions considered to $(u_{\mathrm{rot}}, v_{\mathrm{rot}}) = (-\beta_\epsilon f, 0)$.

In visual space, i.e., xyZ space, that is the space perceived under perspective projection, where the fronto-parallel dimensions are measured according to their size on the image plane, the iso-distortion surfaces take the following form:

$$[x(D-1) + (\hat{x}_0 - Dx_0)]\, n_x + y(D-1)n_y - D\beta_\epsilon f Z n_x = 0$$

That is, they become planes with surface normal vectors $((D-1)n_x, (D-1)n_y, -D\beta_\epsilon f n_x)$. For a fixed D, the family of D iso-distortion surfaces obtained by varying the direction (n_x, n_y) is a family of planes intersecting on a line l. If we slice these iso-distortion planes with a plane parallel to the xy (or image) plane, we obtain a pencil of lines with center lying on the x axis (the point through which line l passes) (see Figure 6a).

In our forthcoming analysis we will need to consider the family of iso-distortion surfaces for a given distortion D, that is, the D iso-distortion surfaces for all directions (n_x, n_y). Thus, we will need a compact representation for the family of D iso-distortion surfaces in 3D space. The purpose of this representation is to visualize the high-dimensional family of D iso-distortion surfaces in $(x, y, Z, \mathbf{n})$ space through a surface in (x, y, Z) space in a way that captures the essential aspects of the parameters describing the family and thus the underlying distortion. As such a representation we choose the following surfaces, hereafter called holistic or H-surfaces, which are most easily understood through their cross sections parallel to the xy plane: Considering a planar slice of

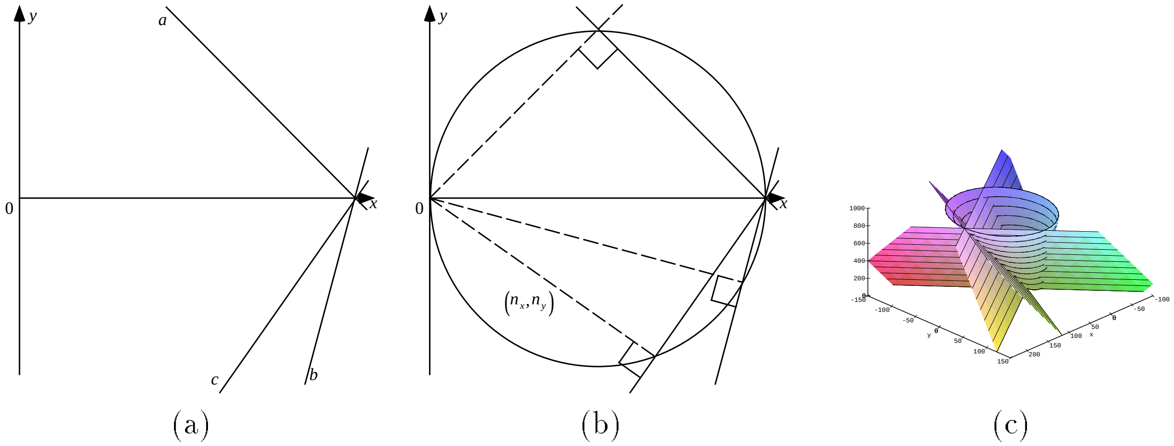

Figure 6: Simplified iso-distortion surfaces in visual space. (a) Intersection of the family of the simplified D iso-distortion surfaces (planes) for different directions (n_x, n_y) with a plane parallel to the image plane. (b) A circle represents the intersections of the family of the D iso-distortion surfaces with planes parallel to the image plane. (c) In visual space a family of D iso-distortion surfaces is characterized by a cone (the holistic surface).

the family of D iso-distortion surfaces, as in Figure 6a, we obtain a pencil of lines. As a representation for these lines we choose the circle with diameter extending from the origin to the center of the pencil (Figure 6b). This circle clearly represents all orientations of the lines of the pencil (or the iso-distortion planes in the slicing plane). Any point P of the circle represents the slice of the iso-distortion plane which is perpendicular to a line through the center (O) and P.

If we now move the slicing plane parallel to itself, the straight lines of the pencil will trace the iso-distortion planes and the circle will change its radius and trace a circular cone with the Z axis as one ruling (Figure 6c).

The circular cones are described by the following equation:

$$\begin{array}{rc} & x^2(D-1) + (\hat{x}_0 - Dx_0)\,x + y^2(D-1) - D\beta_\epsilon f Z x = 0 \\ \text{or} & \left(x - \dfrac{(Dx_0 - \hat{x}_0 + D\beta_\epsilon f Z)}{2(D-1)}\right)^2 + y^2 = \left[\dfrac{D(x_0 + \beta_\epsilon f Z) - \hat{x}_0}{2(D-1)}\right]^2 \end{array}$$

Thus their axes are given by

$$Dx_0 - \hat{x}_0 + D\beta_\epsilon f Z - 2(D-1)x = 0, \quad y = 0$$

Slicing the cones and the simplified iso-distortion surfaces with planes parallel to the xy plane as in Figure 6b, the circles we obtain have center $(x, y, Z) = \left(\frac{Dx_0 - \hat{x}_0 + D\beta_\epsilon f Z}{2(D-1)}, 0, Z\right)$ and radius $\frac{D(x_0 + \beta_\epsilon f Z) - \hat{x}_0}{2(D-1)}$. The circular cones serve as a holistic representation for the family of iso-distortion surfaces represented by the same D, therefore the name holistic or H-surface. It should be noted here that the holistic surfaces become cones only in the case of the constrained 3D motion considered in this paper. In the general case they are hyperboloids.

It must be stressed at this point that the iso-distortion surfaces should not be confused with the H-surfaces. Whereas a D iso-distortion surface for a direction $\mathbf{n}$ represents all points in space distorted by the same multiplicative factor D for image measurements in direction $\mathbf{n}$, the holistic surfaces do not represent any actually existing physical quantity; they serve merely as a tool for visualizing the family of D iso-distortion surfaces as $\mathbf{n}$ varies, and will be needed in explaining the distortion of space due to motion.

The H-surfaces for the families of iso-distortion surfaces vary continuously as we vary D. For $D = 0$ we obtain a cylinder with the Z axis and the line $x = \hat{x}_0$ as diametrically opposite rulings. For $D = 1$ we obtain a plane parallel to the xy plane given by $Z = \frac{-x_{o\epsilon}}{\beta_\epsilon f}$; the cone for $D = \infty$ and the cone for $D = -\infty$ coincide. Thus we can divide the space into three areas: the areas between the $D = 0$ cylinder and the $D = -\infty$ cone, which only contain cones of negative distortion factor; the area between the $D = \infty$ cone and the $D = 1$ plane, with cones of decreasing distortion factor; and the area between the $D = 0$ cylinder and the $D = 1$ plane, with cones of increasing distortion factor. All the holistic surfaces intersect in the same circle, which is the intersection of the $D = 0$ cylinder and the $D = 1$ plane (see Figure 7a). Since the holistic surfaces intersect in one plane, any family of $\mathbf{n}$ iso-distortion surfaces intersects in a line in that plane.

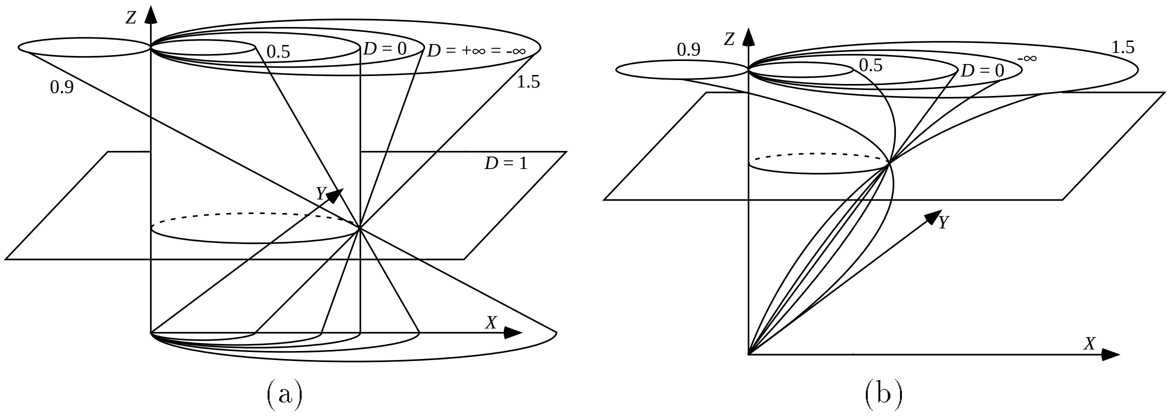

(a) (b)

Figure 7: (a) Holistic surfaces (cones) in visual space, labeled with their respective distortion factors. (b) Holistic surfaces (third-order surfaces) in 3D space.

To go back from visual to actual space, we have to compensate for the perspective scaling. In actual 3D space the iso-distortion surfaces are given by the equation

$$D\beta_\epsilon Z^2 n_x + (1-D)Xn_x + (1-D)Yn_x + (Dx_0 - \hat{x}_0)\frac{Zn_x}{f} = 0$$

describing parabolic cylinders curved in the Z dimension. Also the circular cones have an additional curvature in the Z dimension, and thus the H-surfaces in 3D space are surfaces of the form

$$X^2(D-1)f + Y^2(D-1)f + (\hat{x}_0 - Dx_0)XZ - D\beta_\epsilon XZ^2 f = 0$$

An illustration is given in Figure 7b.

3 Psychophysical Experiments on Depth Perception

In the psychophysical literature a number of experiments has been reported that document a perception of depth which does not coincide with the actual situation. Most of the experiments were devoted to stereoscopic depth perception, using tasks that involved the judgment of depth at different distances. The conclusion usually obtained was that there is an expansion in the perception of depth of near distances and a contraction of depth at far distances. However, most of the studies did not explicitly measure perceived viewing distance, but asked for relative distance judgments instead. Recently a few experiments have been conducted by Tittle et al. [31] comparing aspects of depth judgment due to stereoscopic and monocular motion perception. The experiments were designed to test how the orientations of objects in space and their absolute distances influence the perceptual judgment. It was found that the stereoscopic cue and the motion cue give very different results.

The literature has presented a variety of explanations and proposed a number of models explaining different aspects of depth perception. Recently, great interest has arisen in attempts to explain the perception of visual space using well-defined geometries, such as similarity, conformal, affine, or projective transformations mapping physical space into perceived space, and it has been debated whether perceptual space is Euclidean, hyperbolic, or elliptic [35]. Our analysis shows that these models do not provide a general explanation for depth perception, and proposes that much of the data can be explained by the fact that the underlying 3D transformation is estimated incorrectly. Thus the transformation between physical and perceptual space is more complicated than previously thought. For the case of motion or stereo it is rational and belongs to the family of Cremona transformations [30].

We next describe a number of experiments and show that their results can be explained on the basis of imprecise estimation of the 3D transformation and thus can be predicted by the iso-distortion framework introduced here. Our primary focus in Section 3.1 is on the experiments testing the difference between motion and stereo performed by Tittle et al. [31]. In addition, in Section 3.2 we describe two well-known stereoscopic experiments, and in Section 3.3 a motion experiment.

3.1 Distance Judgment from Motion and Binocular Stereopsis

In the first experiment [31] that we discuss, observers were required to adjust the eccentricity of a cylindrical surface until its cross-section in depth appeared to be circular. The observers could manipulate the cylindrical surface (shown in Figure 8) by rescaling it along its depth extent b (which was aligned with the Z axis of the viewing geometry when the cylinder was in a fronto-parallel orientation) with the workstation mouse. Such a task requires judgment of relative distance. In order for the cross-section to appear circular, the vertical extent and the extent in depth of the cylinder, a and b, have to appear equal.

The experiments were performed for static binocular stereoscopic perception, for monocular motion, and for combined motion and stereopsis. The stereoscopic stimuli consisted of stereograms, and the monocular ones were created by images of cylinders rotating about a vertical axis (see Figure 8). In all the experiments the observers had to fixate on the front of the surface where it intersected the axis of rotation, and the cylindrical surfaces were composed of bright dots.

The effect of the slant and distance of the cylinder on the subjective depth judgment was tested. In particular, the cylinder had a slant in the range 0° to 30°, with 0° corresponding to a fronto-parallel cylinder as shown in Figure 8, and the distance ranged from 70 to 170 cm. Figure 9 displays the experimental results in the form of two graphs, with the x axis showing either the slant or distance and the y axis the adjusted eccentricity. An adjusted eccentricity of 1.0 corresponds to a veridical judgment, values less than this indicate an overestimate of b relative to a, and values greater than 1.0 indicate an underestimate. As can be seen from the graphs, whereas the perception of depth from motion only does not depend on the viewing distance, the extent b is overestimated for near distances and underestimated for far distances under stereoscopic perception. On the other hand, the slant of the surface has a significant influence on the perception of motion—at 0° b is overestimated and at 30° underestimated—and has hardly any influence on perception from stereo. The results obtained from the combined stereo and motion displays showed an overall pattern similar to those of the purely stereoscopic experiments.

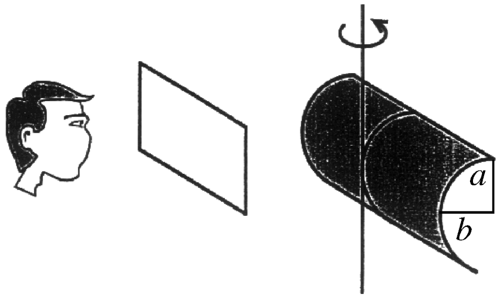

Figure 8: From [31]: a schematic view of the cylinder stimulus used in Experiment 1.

For stereoscopic perception only, a very similar experiment, known as apparently circular cylinder (ACC) judgment, was performed in [13, 18], and the same pattern of results was reported there.

In a second experiment performed by Tittle et al. [31], the task was to adjust the angle between two connected planes until they appeared to be perpendicular to one another (see Figure 10).

Again the surfaces were covered with dots and the fixation point was at the intersection of the two planes and the rotation axis. As in the first experiment the influences of the cue (stereo, motion, or combined motion and stereo), the slant and the viewing distance on the depth judgment were evaluated. This task again requires a judgment of relative distance, that is, the depth extent b relative to the vertical extent a (as shown in Figure 10). The results displayed in Figure 11 are qualitatively similar to those obtained from the first experiment. An adjusted angle greater than the standard 90° corresponds to an overestimation of the extent in depth, and one less than 90° represents underestimation.

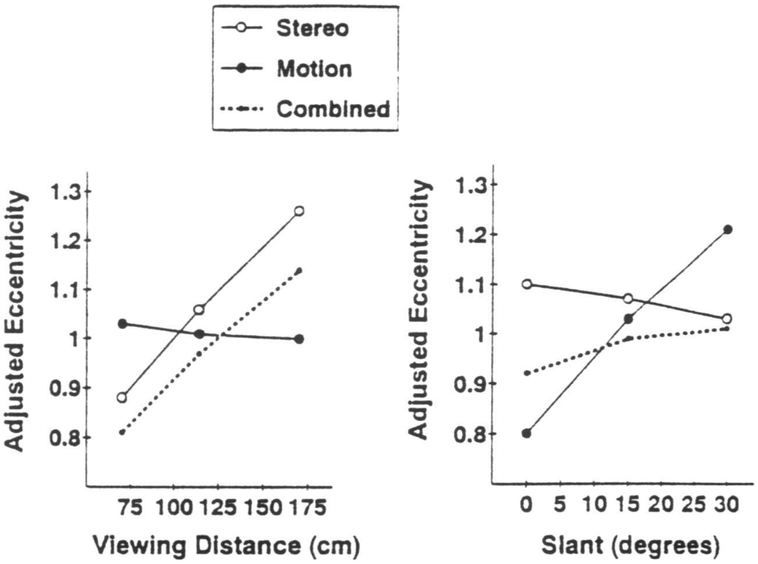

Figure 9: From [31]: Average adjusted cylinder eccentricity for the stereo, motion, and combined conditions as a function of simulated viewing distance and surface slant. An adjusted eccentricity of 1.0 indicates veridical performance.

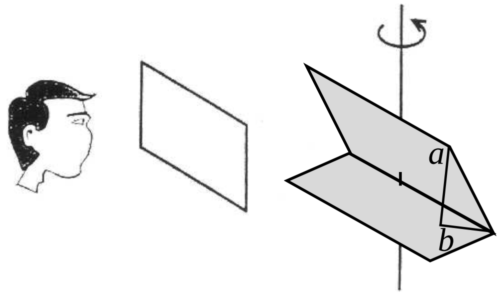

Figure 10: From [31]: a schematic view of the dihedral angle stimulus used in Experiment 2.

3.2 Stereoscopic Experiments: Apparent Fronto-parallel Plane/Apparent Distance Bisection

A classic test of depth perception for stereoscopic vision is the apparent fronto-parallel plane (AFPP) experiment [13, 29]. In this experiment, an observer views a horizontal array of targets. One target is fixed, usually in the median plane (YZ plane). The other targets are fixed in direction but are variable in radial distance under control of the subject. The subject sets these targets so that all of the targets appear to lie in a fronto-parallel plane. Care is taken so that fixation is maintained at one point. The results are illustrated in Figure 12.

The AFPP corresponds to a physical plane only at one distance, usually between 1 m and 4 m [13]. At far distances, the targets are set on a surface convex to the observer; at near distances they are set on a surface increasingly concave to the observer. Generally, the AFPP locus is skewed somewhat, that is, one side is farther away than the other.

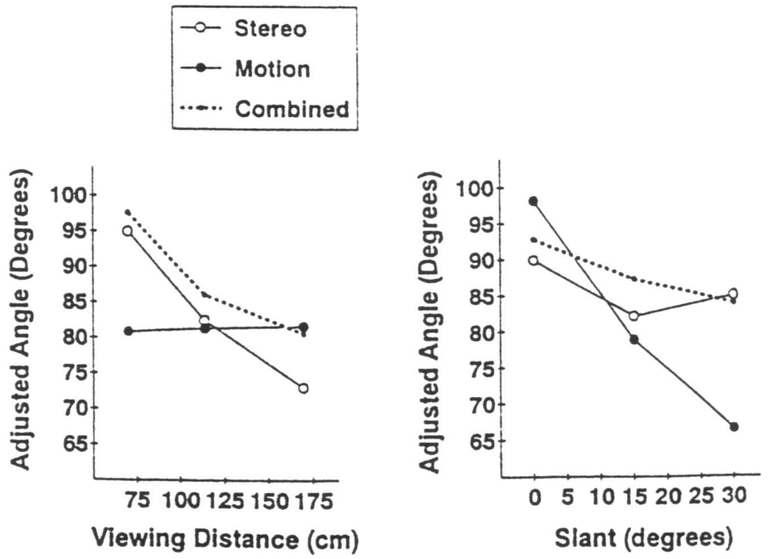

Figure 11: From [31]: Adjusted dihedral angle as a function of surface slant and simulated viewing distance. An adjusted angle of 90° indicates veridical performance.

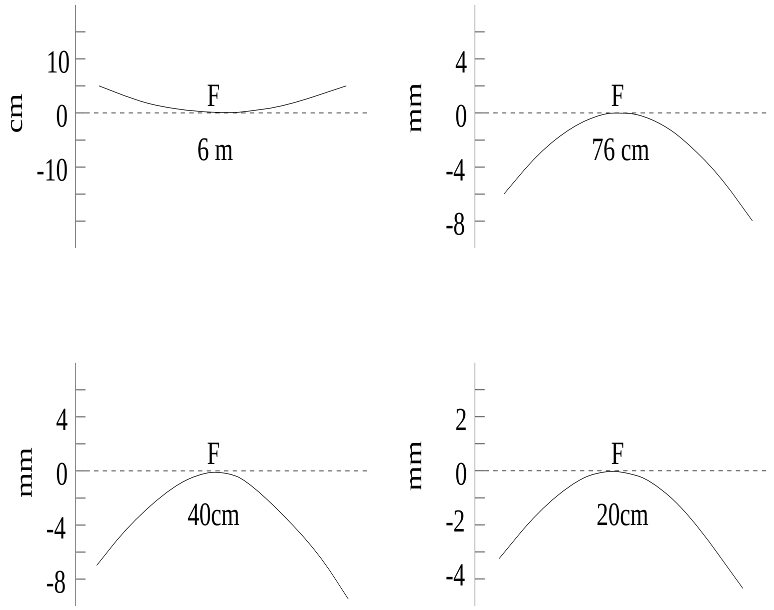

Figure 12: Data for the apparent fronto-parallel plane for different observation distances. In each case, F is the point of fixation. The visual field of the target extends from $-16°$ to $16°$. From [29].

In another classic experiment, instead of instructing a subject to set targets in an apparent fronto-parallel plane, the subjects are asked to set one target at half of the perceived distance of another target, placed in the same direction. This is known as the apparent distance bisection task or the ADB task [12]. In practice the targets would interfere with each other if they were in exactly the same direction, so they are displaced a few degrees. The task and the results are illustrated in Figure 13. These results were obtained with free eye movements, but the author claimed that the effect has also been replicated with fixation on one point.

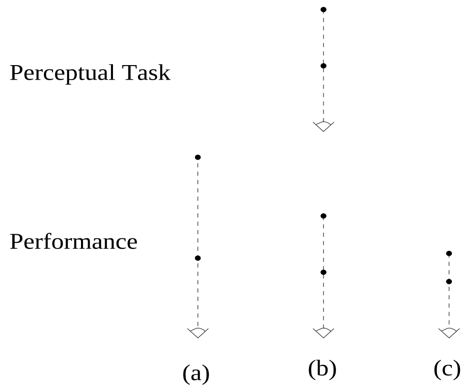

Figure 13: Apparent distance bisection task: (a) Far fixation point. (b) Correct distance judgment at intermediate fixation point. (c) Near fixation point.

3.3 Motion Experiments

In [15], Gogel tested the distance perceived under monocular motion when fixating on points at different distances. In one of his experiments he relates motion to depth in a highly original way. The resulting task can be performed on the basis of scaled depth. The experimental set-up is shown in Figure 14. The subjects sitting in the observation booth moved their heads horizontally while fixating on a point on either a near or far object. Between the two fixation points was a bright, moving point. Imagine the point to be moving vertically. If the distance to the point is estimated correctly the observer experiences a vertical motion. If it is estimated incorrectly the point is perceived as moving diagonally, with a horizontal component either in the direction of the head movement if there is an underestimation of depth, or in the opposite direction if there is an overestimation. In the experiment the subjects controlled the point's movement and were asked to move it in such a way that they experienced a purely vertical movement. To compensate for the additional motion component perceived, subjects moved the point diagonally with a horizontal component in the direction opposite. From the amount of horizontal movement, the estimated depth could be reconstructed. The exact dimensions of the set-up are described in Figure 14. The results of the experiments are displayed in Table 1. As can be seen, overestimation of depth occurs with both fixation points, and it is larger for the far fixation point than for the near one.

4 Explanation of Psychophysical Results

4.1 The Viewing Geometry

(a) Stereo The geometry of binocular projection for an observer fixating on an environmental point is illustrated in Figure 15. We fix a coordinate system $(LXYZ)$ on the

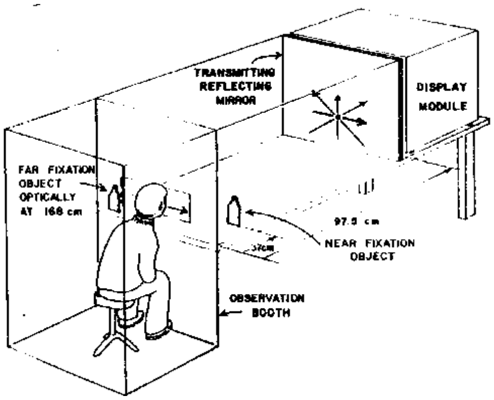

Figure 14: A schematic drawing of the observation booth (from [15]). The observation booth was 50 cm wide and extending optically 194 cm in front of the observer (actually a mirror was used in the display as can be seen). The near fixation object was 15.3 cm from the right edge of the visual alley and 37 cm from the observer. The far fixation object was 2 cm from the left edge of the alley and optically 168 cm from the observer. The moving dot was between the two walls at a distance of 97.5 cm and the observer could move horizontally left and right, in one movement, 17.5 cm. The floor and the two sides of the booth were covered with white dots. All other surfaces were black.

Table 1: Results in centimeters from the experiment shown in Figure 14. W is the physical horizontal motion required for the point of light physically moving with a vertical component to appear to move vertically and D' is the perceived distance of the point of light as derived using the measurement W.

	Fixation Near		Fixation Far	
	W	D'	W	D'
Mean	1.51	117	7.08	164
Geometric Mean	—	112	7.04	164
Median	2.42	113	7.13	165
SD	5.10	34	0.70	11

left eye with the Z axis aligned with the optical axis and the Y axis perpendicular to the fixation plane. In this system the transformation relating the right eye to the left eye is a rotation around the Y axis and a translation in the XZ plane. If we make the small baseline assumption, we can approximate the disparity measurements through a continuous flow field. The translational and rotational velocities are $(U, 0, W)$ and $(0, \beta, 0)$ respectively, and therefore the horizontal h and vertical v disparities are given by

$$\begin{aligned} h &= \tfrac{W}{Z}(x - x_0) & -\beta\left(\frac{x^2}{f} + f\right) \\ v &= \tfrac{W}{Z}y & -\frac{\beta x y}{f} \end{aligned}$$

In the coordinate system thus defined (Figure 15), β is negative and x_0 is positive, and for a typical viewing situation very large. Therefore the epipole is far outside the image plane, which causes the disparity to be close to horizontal.

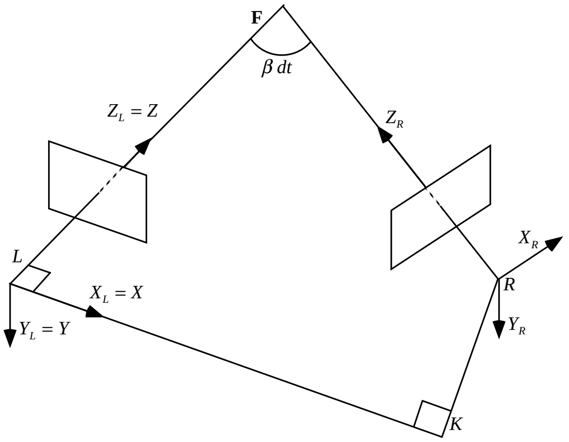

Figure 15: Binocular viewing geometry. $LK = U\,dt$ (translation along the X axis), $KR = W\,dt$ (translation along the Z axis), $LFR = \beta\,dt =$ convergence angle (resulting from rotation around the Y axis). L, K, R, F are in the fixation plane and dt is a hypothetical small time interval during which the motion bringing $X_L Y_L Z_L$ to $X_R Y_R Z_R$ takes place.

(b) Motion In the experiments described in Section 3.1 the motion of the object consists of a rotation around a vertical axis in space.

We fix a coordinate system to a point $S = (X_s, Y_s, Z_s)$ on the object in the YZ plane through which the rotation axis passes. At the time of observation it is parallel to the reference coordinate system $(OXYZ)$ on the eye of the observer (see Figure 16). In the new coordinate system on the object, the motion is purely rotational, and is given by the velocity $(0, w_y, 0)$. If we express this motion in the reference system as a motion of the observer we obtain a rotation around the Y axis and an additional translation in the XZ plane given by the velocity $(w_y Z_s, 0, -w_y X_s)$. Thus in the notation used before, there is a rotation with velocity $\beta = -w_y$, and a translation with epipole $(x_0, 0) = \left(-\frac{Z_s f}{X_s}, 0\right)$ or $(\infty, 0)$ if $X_s = 0$. The value u_n of the flow component $\mathbf{u}_n$ along a direction $\mathbf{n} = (n_x, n_y)$ is given by

$$u_n = w_y \left(\frac{X_s}{Z} \left(x + \frac{Z_s}{X_s} f \right) + \left(f + \frac{x^2}{f} \right) \right) n_x + w_y \left(\frac{y X_s}{Z} + \frac{xy}{f} \right) n_y$$

Since X_s is close to zero, x_0 again takes on very large values. In our coordinate system (see Figure 16) β is positive and x_0 is positive, since the circular cross-section is to the right of the YZ plane, and thus the locus of the fixation point most probably is biased toward the cross-section.

Although the motion in the stereo and motion configurations is qualitatively similar, the psychophysical experimental results show that the system's perception of depth is not.

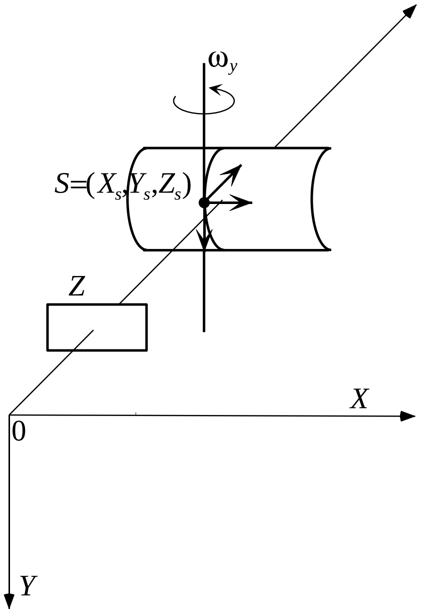

Figure 16:

This demonstrates that the two mechanisms of shape perception from motion and stereo work differently. We account for this by the fact that the 2D disparity representation used in stereo is of a different nature than the 2D velocity representation computed for further motion processing.

It is widely accepted that horizontal disparities are the primary input in stereoscopic depth perception although there have been many debates as to whether vertical disparities play a role in the understanding of shape [19, 28]. The fact is that for any human stereo configuration, even with fixation at nearby points, the horizontal disparities are much larger than the vertical ones. Thus, for the purpose of the forthcoming analysis, in the case of stereo we only consider horizontal disparities, although a small amount of vertical disparity would not influence the results.

On the other hand, for a general motion situation the actual 2D image displacements are in many directions. Due to computational considerations from local image measurements, only the component of flow perpendicular to edges can be computed reliably. This is the so-called aperture problem. In order to derive the optical flow, further processing based on smoothing and optimization procedures has to be performed, which implicitly requires some assumptions about the smoothness of the scene. For this reason we expect the 2D image velocity measurements used by the system to be distributed in many directions, although the optical flow in the experimental motion is mostly horizontal.

Based on these assumptions about the velocity representations used, in the next two sections the experimental data—first the data from motion perception, then the data from stereo perception—are explained through the iso-distortion framework.

4.2 Motion

To visualize this and later explanations let us look at the possible distortions of space for the motion and stereo configurations considered here. Figure 17a gives a sketch of the holistic surfaces (third-order surfaces) for negative rotational errors (β_ϵ) and Figure 17b shows the surfaces for positive rotational errors. In both cases x_0 is positive. A change of the error in translation leaves the structure qualitatively the same; it only affects the sizes of the surfaces. In the overall pattern we observe a shift in the location of the intersection of the holistic surface. Since the intersection is in the $D = 1$ plane given by the equation $Z = -\frac{x_{0_\epsilon}}{\beta_\epsilon f}$, an increase in x_{0_ϵ} causes the intersection to have a smaller Z coordinate in Figure 17a and a larger one in Figure 17b. For both the motion and the stereo experiments, the FOE lies far outside the image plane. Therefore only a small part of the illustrated iso-distortion space actually lies in the observer's field of view. This part is centered around the Z axis as schematically illustrated in Figure 17.

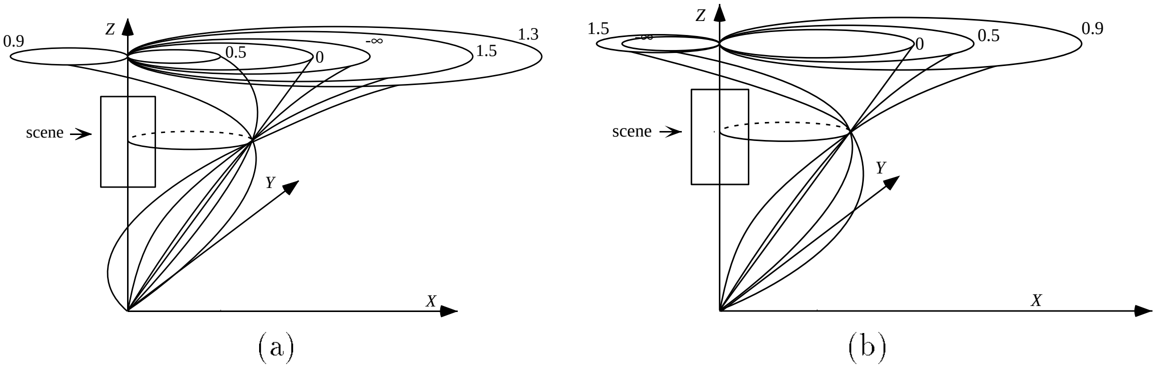

Figure 17: Holistic third-order surfaces for the geometric configurations described in the experiments. (a) Positive β_ϵ. (b) Negative β_ϵ.

The guiding principle in our explanation of the motion experiments lies in the minimization of negative depth estimates. We do not assume any scene interpretation; the only thing we know about the scene is that it lies in front of the image plane, and thus all depth estimates have to be positive. Therefore, we want to keep the number of image points, whose corresponding scene points would yield negative depth values due to erroneous estimation of the 3D transformation, as small as possible.

To represent the negative depth values we use a geometric statistical model: The scene in view lies within a certain range of depths between Z_{min} and Z_{max}. The flow measurement vectors on the image are distributed in many directions; we assume that they follow some distribution. We are interested in the points in space for which we would estimate negative depth values.

For every direction $\mathbf{n}$ the points with negative depths lie between the $D = 0$ and $D = -\infty$ distortion surfaces within the range of depths covered by the scene. Thus, for every gradient direction we obtain a 3D subspace, covering a certain volume. The sum of all volumes for all gradient directions, normalized by the flow distribution considered here, represents a measure of the likelihood of negative depth estimates being derived from the image flow on the basis of some motion estimate. We call this sum the *negative depth volume.*

Let us assume there is some error in the estimate of the rotation, β_ϵ. We are interested in the translation error x_{0_ϵ} that will minimize the negative depth volume. Under the assumption that the distribution of flow directions is uniform (that is, the flow directions are uniformly distributed in every direction and at every depth within the range between $Z_{\min}$ and $Z_{\max}$), and that the simplified model is used (i.e., quadratic terms are ignored) and the computations are performed in visual space, the minimum occurs when the intersection of the iso-distortion cones is at the middle of the depth range of the scene. That is, the $D = 1$ plane is given as $Z = -\frac{x_{0_\epsilon}}{\beta_\epsilon f} = \frac{Z_{\min}+Z_{\max}}{2}$, and $x_{0_\epsilon} = -\beta_\epsilon f \frac{Z_{\min}+Z_{\max}}{2}$ [3].

Of course, we do not know the exact flow distribution, or the exact scene depth distribution, nor do we expect the system to optimally solve a minimization problem. We do, however, expect that the estimation of motion is such that the negative depth volume is kept rather small and thus that x_{0_ϵ} and β_ϵ are of opposite sign and the $D = 1$ plane is between the smallest and largest depth of the object observed.

In the following explanation we concentrate on the first experiment, which was concerned with the judgment about the circular cylinder.

We assume that the system underestimates the value of x_0, because the observer is fixating at the rotation axis in the image center while judging measurements to the right of the center. As this does not correspond to a natural situation (fixation center and object of attention coinciding), the observer should perceive the fixation center closer to the object resulting in an underestimation in the value of x_0. Thus, $x_{0_\epsilon} > 0$ which implies $\beta_\epsilon < 0$ and the distortion space of Figure 17b becomes applicable.

The holistic surfaces corresponding to negative iso-distortion surfaces in the field of view are very large in their circular extent, and thus the flow vectors leading to negative depth estimates are of large slope, close to the vertical direction. Figure 18 shows a cross-section through the negative iso-distortion surfaces and the negative holistic surfaces for a value Z in front of the $D = 1$ plane.

The rotating cylinder constitutes the visible scene. Its vertical cross-section along the axis of rotation lies in the space where x is positive. The most frontal points of the cross-section always lie in front of the $D = 1$ plane, and as the slant of the cylinder increases, the part of the cross-section which lies in front of the $D = 1$ plane increases as well.

The minimization of the negative depth volume and thus the estimation of the motion is independent of the absolute depth of the scene. Therefore a change in viewing distance should not have any effect on the depth perceived by the observer, *which explains the first experimental observation.*

The explanation of the second result lies in a comparison of the estimated vertical extent, $\hat{a}$, and the extent in depth, $\hat{b}$.

Figures 19a–c illustrate the position of the circular cross-section in the distortion space for the fronto-parallel position of the cylinder. Section $a = (AC)$ lies at one depth and intersects the cross section of the holistic surface as shown in Figure 19b. Section $b = (BC)$ lies within a depth interval between depth values Z_B and Z_C. The cross-sections of the holistic surfaces are illustrated in Figure 19c. To make quantitative statements about the distortion D at any depth value, we assume that at any point P,

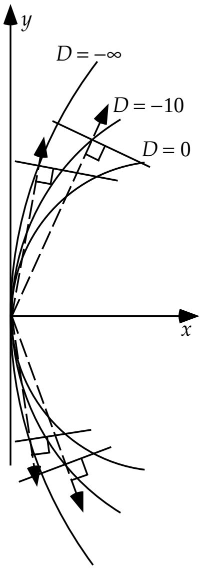

Figure 18: Cross-sections through negative iso-distortion surfaces and negative holistic surfaces. The flow vectors yielding negative depth values have large slopes.

D is the average value of all the iso-distortion surfaces passing through P. With this model we derive $\hat{a}$ and $\hat{b}$ as follows:

$$\hat{a} = Da \tag{5}$$

where D is the average distortion at the depth of section AC. The estimate $\hat{b}$ is derived as the difference of the depth estimate at points B and C. We denote by δ the difference between the average distortion factor of extent a and the distortion at point C, and we use ϵ to describe the change in the distortion factor from point C to point B. Thus

$$\begin{aligned}\hat{b} &= \hat{Z}_C - \hat{Z}_B \\ &= (D+\delta)Z_C - (D+\delta+\epsilon)(Z_C - b) \\ &= (D+\delta)b - \epsilon(Z_C - b) \end{aligned} \tag{6}$$

Z_C is much larger than b and thus $(Z_C - b)$ is always positive. Comparing equations (5) and (6) we see that for $a = b$ the factor determining the relative perceived length of a and b depends primarily on δ and ϵ.

For the case of a fronto-parallel cylinder, where extent a appears behind the $D = 1$ plane, δ is positive (see Figure 19b) and ϵ is negative (see Figure 19c), which means that b will be perceived to be greater than a.

As the cylinder is slanted (see Figures 19d–f), the circular cross-section also becomes slanted. As a consequence the cylinder covers a larger depth range and extent a appears closer to or even in front of the $D = 1$ plane (see Figure 19e). Points on section b have increasing X-coordinates as Z increases (see Figure 19f). As the slant becomes large enough δ reaches a negative value, ϵ reaches a positive value and b is perceived to be smaller than a. Therefore the *results for the experiments involving the cylindrical surface* for the case of motion *can be explained* in terms of the iso-distortion diagrams with D that decreases or increases with Z.

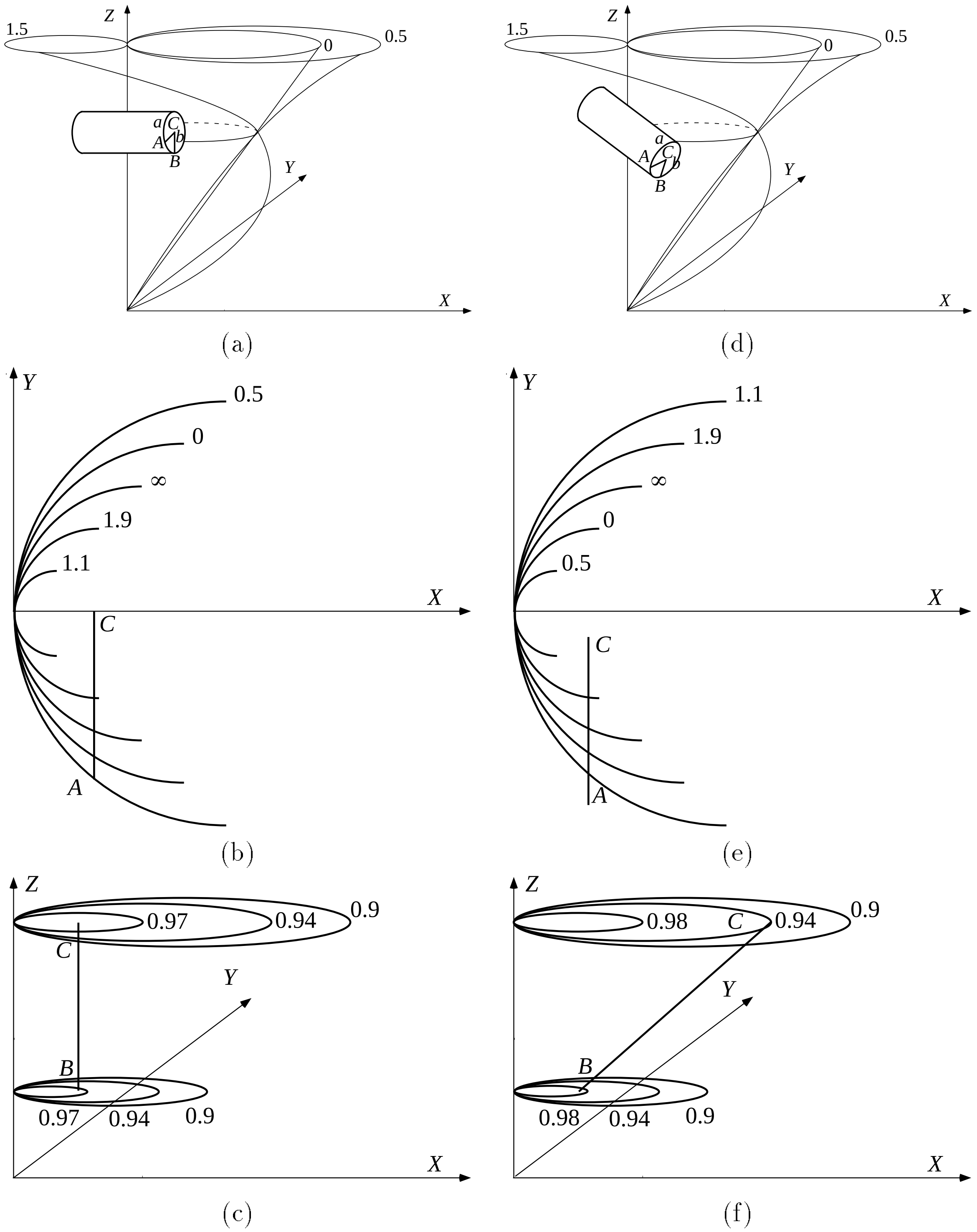
(a) (b) (c) (d) (e) (f)

Figure 19: (a–c) Position of fronto-parallel cylinder in iso-distortion space. (d–f) Position of slanted cylinder in iso-distortion space. The figure shows that extent a appears behind the $D = 1$ plane in (b–c) and in front of the $D = 1$ plane in (e–f).

The second experiment, concerned with the judgment of right angles, can be explained by the same principle. The estimate is again based on judgment of the vertical extent a relative to the extent in depth b (see Figure 10). *Either* we encounter the situation where the sign of x_0 is positive, so that a and b are measured mostly to the right of the YZ plane, and Figure 17b explains the iso-distortion space; *or* x_0 is negative, so that a and b are mostly to the left of the YZ plane, and the iso-distortion space is obtained by reflecting the space of Figure 17b in the YZ plane. In both cases the explanation given for the first experiment still applies. Due to the changes of position of the two planes in iso-distortion space with a change in slant, the extent in depth will be overestimated for the fronto-parallel position and underestimated for larger slants.

4.3 Stereo

In the case of stereoscopic perception the primary 2D image input is horizontal disparity. Due to the far-off location of the epipole the negative part of the distortion space for horizontal vectors does not lie within the field of view, as can be seen from Figure 17.

Since depth estimation in stereo vision has long been of concern to researchers in psychophysics, a large amount of experimental data has been published, and the parameters of the human viewing geometry are well documented. In [13] Foley studied the relationship between viewing distance and error in the estimation of convergence angle (β in our notation). From experimental data he obtained the relationship between perceived convergence angle and actual convergence angle shown in Figure 20.

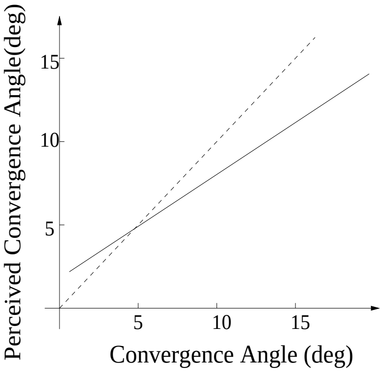

Figure 20: Perceived convergence angle as a function of convergence angle.

According to his data, the convergence angle is overestimated at far distances and underestimated at near distances. Foley expressed the data through the following relationship:

$$-\hat{\beta} = E + G(-\beta)$$

with E and G in the vicinity of 0.5; in the figures displayed here the following parameters based on data of Ogle [29] have been chosen: $E = 0.91°$ and $G = 0.66°$.

On the basis of these data, models have been proposed [12, 13, 29] that explain the perception of concavity and convexity for objects in a fronto-parallel plane. To account for the skewing described in the AFPP task an additional model has been employed which assumes the ocular images are of different sizes.

In our explanation we use the experimental data of Figure 20 to explain β_ϵ. As will be shown, the iso-distortion framework alone allows us to explain all aspects of the experimental findings. For far fixation points β_ϵ is positive (since $\beta < 0$) and the iso-distortion space of Figure 17a applies. If we also take into account the quadratic term in the horizontal disparity formula of Section 4.1(a) (that is, the rotational part $\beta_\epsilon(\frac{x^2}{f}+f)$), we obtain an iso-distortion configuration for horizontal vectors as shown in Figure 21. In particular Figure 21a shows the contours obtained by intersecting the iso-distortion surfaces with planes parallel to the xZ plane in visual space, and Figure 21b shows the same contours in actual 3D space. Irrespective of x_{0_ϵ} the iso-distortion factor decreases with depth Z. The sign of x_{0_ϵ} determines whether the $D = 1$ contour (the intersection of the $D = 1$ surface with the xZ plane) is in front of or behind the image plane, and the exact position of the object with regard to the $D = 1$ contour determines whether the object's overall size is over- or underestimated.

For near fixation points, β_ϵ is negative and the iso-distortion space appears as in Figure 17b. The corresponding iso-distortion contours derived by including the quadratic term are illustrated in Figure 21c and d.

The perceived estimates $\hat{a}$ and $\hat{b}$ are modeled as before. However, this time it is not necessary to refer to an average distortion D, since only one flow direction is considered. Section a lies in the yZ plane and $\hat{a}$ is estimated as aD, with D the distortion factor at point C. The estimate for b is

$$\hat{b} = Db - \epsilon(Z_C - b)$$

As can be seen from Figures 21a and c, ϵ is increasing if the fixation point is distant and decreasing if the fixation point is close, and we thus obtain the under- and overestimation of $\hat{b}$ as experimentally observed. A slanting of the object has very little effect on the distortion pattern because the fixation point is not affected by it. As long as the slant is not too large, causing ϵ to change sign, the qualitative estimation of depth should not be affected by a change in slant. The slant might, however, influence the amount of over- and underestimation. There should be a decrease in the estimation error as the slant increases, since section b covers a smaller range of the distortion space. This can actually be observed from the experimental data in Figure 9.

The same explanation covers the second experiment related to the judgment of angles.

4.4 Explanation of Purely Stereoscopic and Purely Motion Experiments

The iso-distortion patterns outlined in Section 4.3 also explain the purely stereoscopic experiments. With regard to the AFPP task it can be readily verified that the iso-distortion diagram of Figure 21a (far fixation point) causes a fronto-parallel plane to appear on a concave surface, and thus influences the observer to set them at a convex AFPP locus, whereas the diagram of Figure 21c (near fixation point) influences the observer to set them on a concave AFPP locus. In addition, the skewing of the AFPP loci is also predicted by the iso-distortion framework.

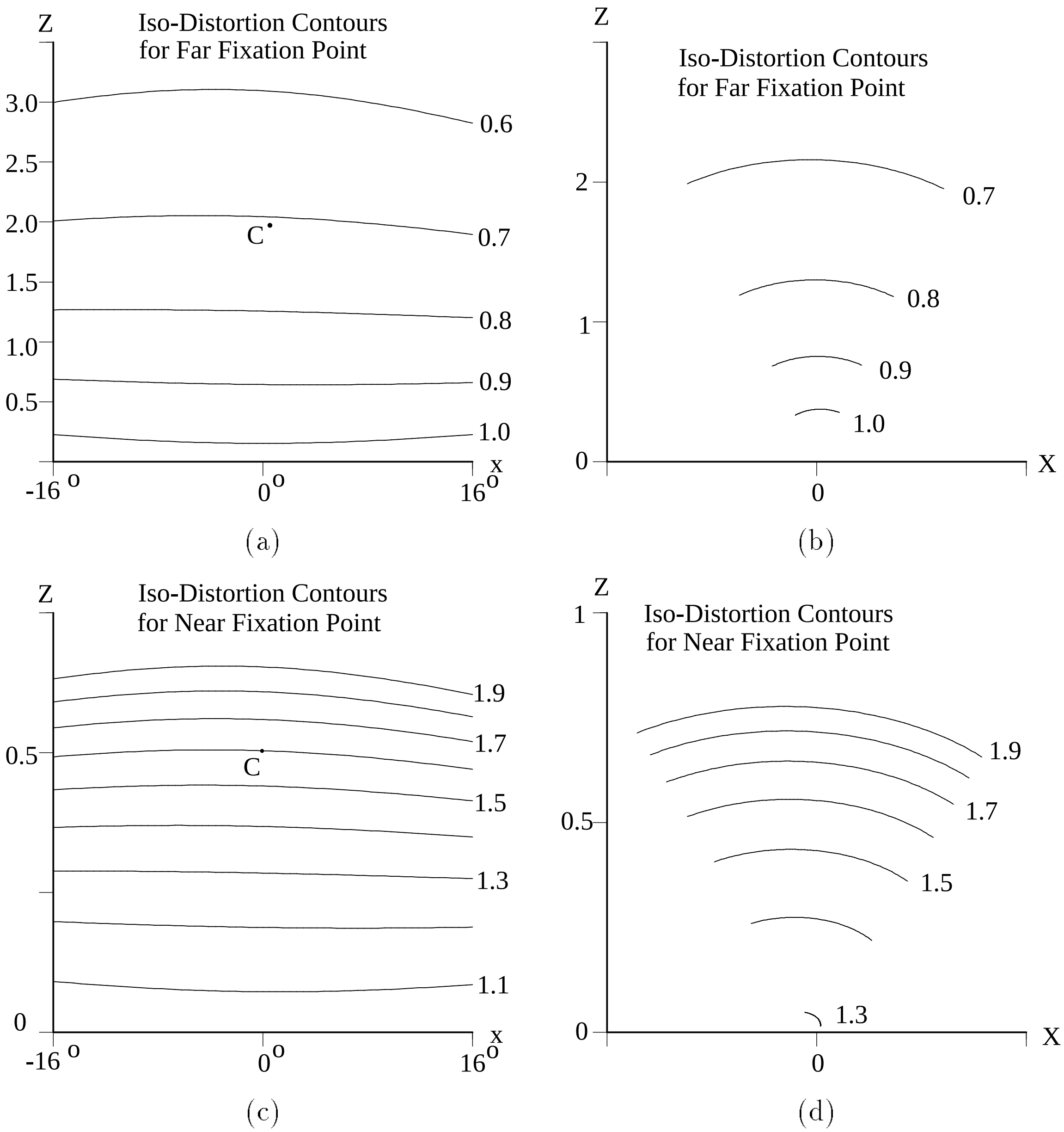

(a)

(b)

(c)

(d)

Figure 21: Iso-distortion contours for horizontal disparities: (a, b) for far fixation point in visual space (a) and actual space (b); (c, d) for near fixation point in visual and actual space.

With regard to the ADB task, the iso-distortion patterns predict that the target will be set at a distance closer than half-way to the fixation point if the latter is far, and at a distance further than half-way to the fixation point if the latter is near, which is in agreement with the results of the task.

In the motion experiment of [15] the 3D motion parameters are as follows. When fixating on one of the two objects the z axis passes through the fixation point, the translation of the observer's head is along the x axis, the rotation of the observer's head (due to fixation) is around the y axis, and the vertical motion component of the point is parallel to the y axis. The scene in view is the observation booth covered with dots.

When the observer fixates on the near point $x_0 > 0$. As in the experiments in Section 4.2, it is assumed that the value of x_0 is underestimated, that is, $\hat{x_0} < x_0$, and $\beta_\epsilon < 0$. The resulting distortion space corresponds to the one sketched in Figure 17b. The moving point appears to the left of the YZ plane, and since the observer fixates on a point in the front part of the scene, it should be behind the $D = 1$ plane. The flow vectors originating from the movement of the point are in a diagonal direction. As can be seen, in the area of the moving point the distortion for that direction is greater than one, and thus the distance of the point is overestimated. When the observer fixates on the far point $x_0 < 0$. If again the absolute value of x_0 is underestimated, $\hat{x_0} > x_0$ and $\beta_\epsilon > 0$. The distortion space is the one we obtain by reflecting the space of Figure 17a in the YZ plane. In this reflected space the moving point appears to the right of the YZ plane and since the observer fixates on a point in the back of the scene, it should be in front of the $D = 1$ plane. In this area too there occurs an overestimation of distances. This explains the general overestimation found in [15].

In order to assess the exact amount of overestimation we would need to know a number of parameters exactly. The estimated motion, the exact position of the point in the distortion space, and the estimated flow directions determine the distortion factor. Our intuitive argument is as follows. It can be seen that the negative distortion space in Figure 17b behind the $D = 1$ plane increases very quickly with the distance from the plane. It is therefore assumed that the moving point lies closer to the $D = 1$ plane for the near fixation than for the far fixation, and thus the distortion should be smaller for the near fixation than for the far one, as observed in the experiment.

5 Conclusions

The geometric structure of the visual space perceived by humans has been a subject of great interest in philosophy and perceptual psychology for a long time [2, 23, 24, 29]. With the advent of digital computers and the possibility of constructing anthropomorphic robotic devices that perceive the world in a way similar to the way humans and animals perceive it, computational studies are beginning to be devoted to this problem [20].

Many synthetic models have been proposed over the years in an attempt to account for the systematic distortion between physical and perceptual space. These range from Euclidean geometry [14] to hyperbolic [24] and affine [32, 35] geometry. Many other interesting approaches have also been proposed, such as the Lie group theoretical studies of Hoffman [16] and the work of Koenderink and van Doorn [21], that are characterized by a deep geometric analysis concerned with the invariant quantities of the distorted perceptual space. It is generally believed in the biological sciences that a large number of shape representations are computed in our heads and different cues are processed with different algorithms. For the case of motion and/or stereo, there might exist more than one process performing local analysis of motion or stereo disparity, that might work at several levels of resolution [25]. The analysis proposed here has concentrated on a global examination of motion or disparity fields to explain a number of psychological results about the distortion of visual space that takes place over an extended field of view.

In contrast to the synthetic approaches in the literature, we have offered an analytic account of a number of properties of perceptual space. Our starting point was the fact that when we have multiple views of a scene (motion or stereo), then the 3D rigid transformation relating the views, and functions of local image correspondence, determine the perceived depth of the scene. However, even slight miscalculations of the parameters of the 3D transformation result in computing a distorted version of the actual physical space. In this paper, we studied geometric properties of the computed distorted space. We have concentrated on analyzing the distortions from first principles, through an understanding of iso-distortion loci, and introduced an analytic, geometric framework as a tool for modeling the distortion of depth.

It was found that, in general, the transformation between physical and perceptual space (i.e., actual and computed space) is a Cremona transformation; however, it turns out that this transformation can be approximated locally quite closely by an affine transformation in the inverse depth or a hyperbolic transformation in the depth. This can be easily understood from the equations. For the case of stereo, where $n_x = 1$, if we ignore the quadratic terms in the image coordinates which are very small with regard to the linear and constant terms, we obtain from equation (3)

$$\hat{Z} = Z \cdot \frac{x - \hat{x}_0}{x - x_0 + \beta_\epsilon f Z} \qquad \text{or}$$

$$\frac{1}{\hat{Z}} = \frac{\frac{x - x_0}{Z} + \beta_\epsilon f}{x - \hat{x}_0} \tag{7}$$

If we consider x to be locally constant equation (7) describes $\hat{Z}$ locally as a hyperbolic function of Z or $1/\hat{Z}$ as an affine function of $1/Z$.

Thus our model is in accordance with some of the models previously employed in the psychophysical literature. For all practical purposes the locally described approximations are so close to the real Cremona transformation that they cannot possibly be distinguished from experimental data.

Finally, in the light of the misperceptions arising from stereopsis and motion, the question of how much information we should expect from these modules must be raised. The iso-distortion framework can be used as an avenue for discovering other properties of perceived space. Such properties may lead to new representations of space that can be examined through further psychophysical studies. We are interested ultimately in the invariances of the perceived distorted space, since these invariances will reveal the nature of the representations of shape that flexible vision systems, biological or artificial, extract from images.

References

[1] J. Y. Aloimonos and D. Shulman. Learning early-vision computations. *Journal of the Optical Society of America A*, 6:908–919, 1989.

[2] A. Ames, K. N. Ogle, and G. H. Glidden. Corresponding retinal points, the horopter and the size and shape of ocular images. *Journal of the Optical Society of America A*, 22:538–631, 1932.

[3] L. Cheong, C. Fermüller, and Y. Aloimonos. Interaction between 3D shape and motion: Theory and applications. Technical Report CAR-TR-773, Center for Automation Research, University of Maryland, June 1996.

[4] K. Daniilidis. *On the Error Sensitivity in the Recovery of Object Descriptions.* PhD thesis, Department of Informatics, University of Karlsruhe, Germany, 1992, in German.

[5] K. Daniilidis and H. H. Nagel. Analytical results on error sensitivity of motion estimation from two views. *Image and Vision Computing*, 8:297–303, 1990.

[6] K. Daniilidis and M. E. Spetsakis. Understanding noise sensitivity in structure from motion. In Y. Aloimonos, editor, *Visual Navigation: From Biological Systems to Unmanned Ground Vehicles*, chapter 4. Lawrence Erlbaum Associates, Hillsdale, NJ, 1997.

[7] O. D. Faugeras. *Three-Dimensional Computer Vision.* MIT Press, Cambridge, MA, 1992.

[8] C. Fermüller and Y. Aloimonos. Direct perception of three-dimensional motion from patterns of visual motion. *Science*, 270:1973–1976, 1995.

[9] C. Fermüller and Y. Aloimonos. Algorithm independent stabiity analysis of structure from motion. Technical Report CAR-TR-840, Center for Automation Research, University of Maryland, 1996.

[10] C. Fermüller and Y. Aloimonos. Ordinal representations of visual space. In *Proc. ARPA Image Understanding Workshop*, pages 897–903, February 1996.

[11] C. Fermüller and Y. Aloimonos. Towards a theory of direct perception. In *Proc. ARPA Image Understanding Workshop*, pages 1287–1295, February 1996.

[12] J. M. Foley. Effects of voluntary eye movement and convergence on the binocular appreciation of depth. *Perception and Psychophysics*, 11:423–427, 1967.

[13] J. M. Foley. Binocular distance perception. *Psychological Review*, 87:411–434, 1980.

[14] J. J. Gibson. *The Perception of the Visual World.* Houghton Mifflin, Boston, 1950.

[15] W. C. Gogel. The common occurrence of errors of perceived distance. *Perception & Psychophysics*, 25(1):2–11, 1979.

[16] W. C. Hoffman. The Lie algebra of visual perception. *Journal of Mathematical Psychology*, 3:65–98, 1966.

[17] B. K. P. Horn. *Robot Vision.* McGraw Hill, New York, 1986.

[18] E. B. Johnston. Systematic distortions of shape from stereopsis. *Vision Research*, 31:1351–1360, 1991.

[19] R. Julesz. *Foundations of Cyclopean Perception.* University of Chicago Press, Chicago, IL, 1971.

[20] J. J. Koenderink and A. J. van Doorn. Two-plus-one-dimensional differential geometry. *Pattern Recognition Letters*, 15:439–443, 1994.

[21] J. J. Koenderink and A. J. van Doorn. Relief: Pictorial and otherwise. *Image and Vision Computing*, 13:321–334, 1995.

[22] S. Kosslyn. *Image and Brain.* MIT Press, Cambridge, MA, 1993.

[23] J. M. Loomis, J. A. D. Silva, N. Fujita, and S. S. Fukusima. Visual space perception and visually directed action. *Journal of Experimental Psychology*, 18(4):906–921, 1992.

[24] R. K. Luneburg. *Mathematical Analysis of Binocular Vision.* Princeton University Press, Princeton, NJ, 1947.

[25] H. A. Mallot, S. Gillner, and P. A. Arndt. Is correspondence search in human stereo vision a coarse-to-fine process? *Biological Cybernetics*, 74:95–106, 1996.

[26] D. Marr. *Vision.* W.H. Freeman, San Francisco, CA, 1982.

[27] S. J. Maybank. *Theory of Reconstruction from Image Motion.* Springer, Berlin, 1993.

[28] J. E. W. Mayhew and H. C. Longuet-Higgins. A computational model of binocular depth perception. *Nature*, 297:376–378, 1982.

[29] K. N. Ogle. *Researches in Binocular Vision.* Hafner, New York, 1964.

[30] J. G. Semple and L. Roth. *Inroduction to Algebraic Geometry.* Oxford University Press, Oxford, United Kingdom, 1949.

[31] J. S. Tittle, J. T. Todd, V. J. Perotti, and J. F. Norman. Systematic distortion of perceived three-dimensional structure from motion and binocular stereopsis. *Journal of Experimental Psychology: Human Perception and Performance*, 21:663–678, 1995.

[32] J. T. Todd and P. Bressan. The perception of three-dimensional affine structure from minimal apparent motion sequences. *Perception and Psychophysics*, 48:419–430, 1990.

[33] R. Y. Tsai and T. S. Huang. Uniqueness and estimation of three-dimensional motion parameters of rigid objects with curved surfaces. *IEEE Transactions on Pattern Analysis and Machine Intelligence*, 6:13–27, 1984.

[34] H. L. F. von Helmholtz. *Treatise on Physiological Optics*, volume 3. Dover, 1962. J. P. C. Southhall, trans. Originally published in 1910.

[35] M. Wagner. The metric of visual space. *Perception and Psychophysics*, 38:483–495, 1985.